

# **Understanding Sensorless Vector Control for Brushless DC Motors**

Huangsheng Xu, Ph. D. & Yashvant Jani, Ph. D.  
Sr. Staff Applications Engineer & Director of MPU Application Engineering  
Renesas Technology America  
[huangsheng.xu@renesas.com](mailto:huangsheng.xu@renesas.com)  
[yashvant.jani@renesas.com](mailto:yashvant.jani@renesas.com)  
Class #: ESC-543  
Embedded Systems Silicon Valley 2008

## Table of Contents

<b>1. Introduction</b> .....	3
<b>2. BLDC Motors and Vector Control</b> .....	4
<b>3. Sensorless Vector Control with DCCT Measurements</b> .....	11
<b>4. Sensorless Vector Control With One-shunt Current Detection Method</b> .....	14
<b>5.1 Comparison of Cost and CPU Bandwidth</b> .....	17
<b>5.2 Comparison of Motor Phase Currents</b> .....	19
<b>5.3 Comparison of Speed Response and Regulation</b> .....	20
<b>6. Summary</b> .....	22

---

---

# Understanding Sensorless Vector Control for Brushless DC Motors

Huangsheng Xu, Ph. D. & Yashvant Jani, Ph. D.  
Sr. Staff Applications Engineer & Director of MPU Application Engineering  
Renesas Technology America  
[huangsheng.xu@renesas.com](mailto:huangsheng.xu@renesas.com)  
[yashvant.jani@renesas.com](mailto:yashvant.jani@renesas.com)

Class #: ESC-543  
Embedded Systems Silicon Valley 2008

---

---

## Abstract:

This seminar covers sensorless vector control formulation for brushless DC (BLDC) motors and related implementation techniques. We start with basic theory in terms of the BLDC motor model, vector control principles, Clark and Park transformation, pulse-width modulation (PWM), and speed and position estimation. Next, vector control based on the sensor and its normal processing is briefly explained. Then we focus on a processing method for vector control that does not use position or speed sensors. A specific implementation of the motor-model-based flux observer and an overall implementation strategy for sensorless vector control are described, as are techniques for measuring currents via conventional sensors or one-shunt reconstruction. Finally, we present data on the performance of sensorless vector control in terms of speed regulation and CPU bandwidth usage.

## 1. Introduction

Many researchers and engineers have dedicated their efforts to developing and applying methods of vector control — and sensorless vector control, which eliminates the speed sensor — for use in various industries [1,2,3,4]. Manufacturers such as ABB, Allen-Bradley, Hitachi, Mitsubishi, Siemens, and others have marketed vector drives and sensorless vector drives. Appliance manufacturers also have tried to put sensorless vector control of three-phase AC motors into practice [5,6]. However, until recently several factors prevented these advanced motor control techniques from gaining widespread acceptance: (1) the complicated theoretical mathematical modeling, (2) the involved implementation strategy, and (3) the lack of cost-effective, high-performance microcontrollers (MCUs) and digital signal processors (DSPs).

Today fast, low-cost MCUs are readily available, and implementing advanced motor control schemes into digitized high-performance motor control systems has become much easier. Vector control — in particular, sensorless vector control — has become popular and many design groups are implementing sensorless vector control of three-phase permanent magnet synchronous motors (PMSMs).

Vector control, through coordinate transformation, decouples three-phase stator currents into two-phase dq-axis rotor currents, one that produces flux and the other that produces torque. Such a formulation makes it possible to control motor flux and torque directly (similar to a DC motor) so that fast dynamic response and excellent steady-state performance can be achieved.

The sensorless vector control formulation makes estimates of the motor's speed and the position of the rotor from the observed stator currents. It removes the speed sensor (typically an encoder) from the design and reduces the cost. The cost savings are the main reason why consumer appliance manufacturers are interested in this control method.

To be sure, the general formulation of sensorless vector control also uses two high-side current sensors for measuring phase currents, and those sensors do contribute to the cost of the overall drive system. Alternatively, though, the phase currents can be measured with a precision shunt resistor using the one-shunt current detection (OSCD) technique if the MCU incorporates a special timer unit. This approach achieves a further reduction in drive system cost because that shunt resistor is much less expensive than the two high-side current sensors.

Renesas has developed two versions of sensorless vector control: One uses two high-side DCCT current sensors, while the other uses one low-side shunt resistor and an OSCD current measurement technique. Both versions have been implemented using a 32-bit SuperH RISC microcontroller, and we have evaluated the performance of both control techniques in the laboratory.

In this seminar, we begin by discussing the basic formulation of vector control in section 2, and then describe the flux calculations and angle observer for DCCT-based vector control in section 3. The OSCD formulation is described in section 4. In section 5, we present the results of out lab tests of the two versions of sensorless vector control. A summary is provided in section 6.

## **2. BLDC Motors and Vector Control**

A brushless DC motor has two main components: a rotor made up of permanent magnets and a stator with a winding connected to the control electronics. This implementation eliminates the brushes and commutation ring of a universal-type AC motor. Instead, it uses control electronics to generate a proper sequence for commutation. Because of its design, the BLDC motor is also known by several other names: permanent magnet synchronous motor (PMSM), brushless permanent magnet motor, or permanent magnet AC (PMAC) motor. Sometimes it's simply called a PM motor.

The stator of the BLDC motor has three sets of coils. They are known as A, B and C, as shown in Figure 1. When current is passed through two coils (the A and B pair), it generates a magnetic field with a polarity that creates torque on the central magnet—in this case, the rotor. When current is passed in a certain direction, the central rotor rotates clockwise. When the rotor reaches a predetermined position, current is switched from one coil to another coil. (Instead of the A-B pair, current passes through the A-C pair.) The result is that the torque continues in the same direction. When the rotor advances to another specific position, current is again switched to another coil pair, and the generation of torque continues. The process of switching the coils, called commutation, is performed by the MCU and semiconductor power switching devices (MOSFETs and IGBTs) in the electronics of the BLDC motor.

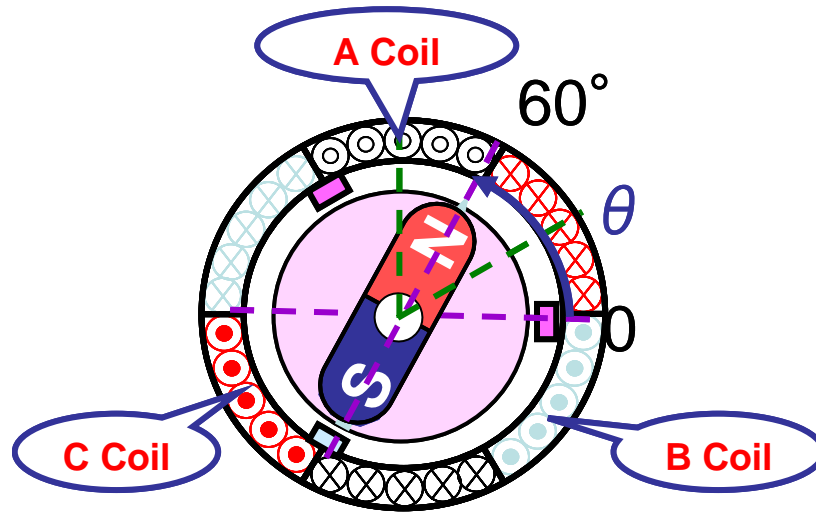


Fig. 1 Typical 3-phase BLDC motor has six stator coils and a permanent magnet rotor.

The basic technique of BLDC control is known as the 120-degree six-step method, in which only two coils are used. Current is modulated as necessary to maintain the proper speed of the rotor. This technique has torque ripple issue that limit control performance. An alternate method, 180-degree modulation, creates smooth torque by energizing all three coils simultaneously with complimentary PWM outputs. With this method, torque ripple can be reduced when vector formulation is used. An advantage of the vector formulation is that the torque and flux are controlled properly as a function of single current value, similar to a DC motor formulation.

As part of our discussion, we will show how the vector control formulation allows torque and flux to be controlled in a direct way. Then we will use the same formulation to derive a sensorless formulation that estimates the speed and angle based on the stator currents measured and voltages applied. Later, we will introduce a new method to measure three currents via a single shunt resistor.

In the abc stationary frame, the model of a three-phase PMSM motor [1,2,3,4,7] can be described as

$$V_{abc_s} = \Lambda_s i_{abc_s} + \frac{d}{dt} \lambda_{abc_s} \quad (1)$$

where  $\Lambda_s = \text{diag}[r_s \quad r_s \quad r_s]$  is the stator resistance matrix and  $\lambda_{abc_s}$  is the stator flux. Stator frame is denoted by the suffix “s,” and each coil is denoted by the suffix “abc.”

The flux linkage equation can be expressed as

$$\lambda_{abcS} = L_S i_{abcS} + \lambda_m \begin{bmatrix} \sin \theta_r \\ \sin(\theta_r + \frac{2\pi}{3}) \\ \sin(\theta_r - \frac{2\pi}{3}) \end{bmatrix} \quad (2)$$

where  $L_S$  is the stator self-inductance matrix,  $\lambda_s$  is the stator flux matrix, and  $\lambda_m$  denotes the amplitude of the flux linkages established by the permanent magnet. Here  $\theta_r$  is the rotor angle with respect to the stator reference frame denoted by abc.

The electromagnetic torque can be written as

$$T_e = \frac{P}{2} \lambda_m [(i_{as} - \frac{1}{2}i_{bs} - \frac{1}{2}i_{cs}) \cos \theta_r - \frac{\sqrt{3}}{2}(i_{bs} - i_{cs}) \sin \theta_r] + T_{cog}(\theta_r) \quad (3)$$

The  $P$  is number of pole pairs, and  $T_{cog}(\theta_r)$  represents the cogging torque. Current in each coil is denoted by its suffix: a, b, or c.

Thus, the motor equations are nonlinear. Moreover, they're strongly coupled with each other. These factors make it very difficult to perform direct control of flux and torque by varying the currents in the coils.

The goals of vector control formulation are to transfer these nonlinear equations into linear equations and decouple the three-phase stator currents into a flux component and a torque component. When this is done, torque and flux can be controlled directly, in the same way that it's done to control a separately excited DC motor. In fact, the vector control uses vector equations and rotor orientation to transform the coupled three-phase AC motor model into a linear model that's very similar to the linear motor model of DC motor. It enables the performance of BLDC motor drives to be comparable or even superior to that of DC motor drives.

Vector control offers multiple benefits:

- Transformation of a complicated, coupled AC motor model into a simple linear system
- Direct control of flux and torque, similar to a DC motor
- Fast dynamic response and good transient and steady-state performance
- High torque and low current at startup
- High efficiency
- Wide speed range by directly weakening the flux.

Vector control establishes three reference frames:

1. Stator reference frame ( $a, b, c$ ) in which the a, b and c axes are co-planar, at 120 degrees to each other;
2. An orthogonal reference frame ( $\alpha\beta$ ) in the same plane as the stator reference frame so that the angle between the two axes is 90 degrees instead of 120 degrees. The  $a$  axis is aligned with  $\alpha$  axis in the second frame;

3. A rotor frame, known as the ( $dq$ ) frame, in which the d axis is along the N and S poles or along the flux vector of the rotor, and the q axis is at 90 degrees to the d axis. Thus, the  $dq$  reference frame is also an orthogonal reference frame.

Figure 2 shows all three frames. The first transformation  $abc \rightarrow \alpha\beta$  is known as the Clark transformation. It is given by equation 4 below. The second transformation  $\alpha\beta \rightarrow dq$  is known as Park transformation and is given by equation 5, as shown in Figure 2. Here  $F$  is Magneto Motive Force, and  $\theta$  is the angle between the d-axis and the  $\alpha$ -axis, also known as the rotor angle.

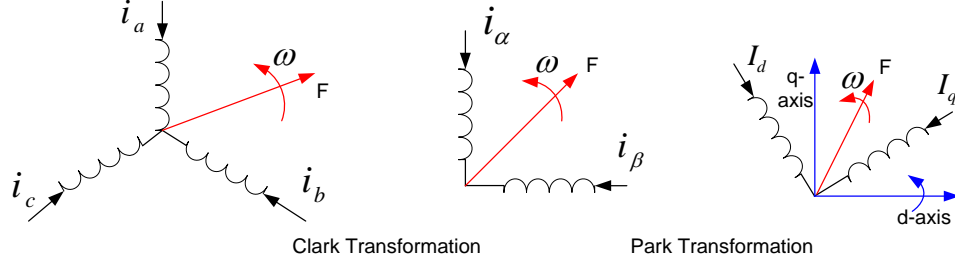


Fig. 2 Clark and Park transformations.

The projection of the stator current vectors in the  $\alpha\beta$  frame is given by equation (4):

$$\begin{bmatrix} i_\alpha \\ i_\beta \end{bmatrix} = \begin{bmatrix} 1 & -\frac{1}{2} & -\frac{1}{2} \\ 0 & \frac{\sqrt{3}}{2} & -\frac{\sqrt{3}}{2} \end{bmatrix} \begin{bmatrix} i_a \\ i_b \\ i_c \end{bmatrix} \quad (4)$$

The Clark transformation converts the three balanced  $abc$  currents into two phase-balanced  $\alpha\beta$  currents. In the  $\alpha\beta$  frame, the expression of torque still depends on the position of the rotor flux, preventing any easy solution of the electrical differential equation. To remove this dependency, the Park transformation is adopted in a two-phase  $dq$  system (as shown in Figure 2) that rotates at the electrical speed of the rotor, and the d axis is aligned with the electrical position of the rotor flux. In the  $dq$  frame, the electrical expression of the torque becomes independent from the rotor position.

The equations corresponding to this transformation are given by

$$\begin{bmatrix} I_d \\ I_q \end{bmatrix} = \begin{bmatrix} \cos \theta & \sin \theta \\ -\sin \theta & \cos \theta \end{bmatrix} \begin{bmatrix} i_\alpha \\ i_\beta \end{bmatrix}. \quad (5)$$

The three-phase PMSM motor model (described in equations 1-3) can be transformed from the  $abc$  stator frame into the  $dq$  frame as follows:

$$V_{ds} = r_s i_{ds} - \omega_r \lambda_{qs} + \frac{d}{dt} \lambda_{ds} \quad (6)$$

$$V_{qs} = r_s i_{qs} + \omega_r \lambda_{ds} + \frac{d}{dt} \lambda_{qs} \quad (7)$$

$$\lambda_{ds} = L_s i_{ds} + \lambda_m \quad (8)$$

$$\lambda_{qs} = L_s i_{qs} \quad (9)$$

$$T_e = \frac{3}{2} p (\lambda_{ds} i_{qs} - \lambda_{qs} i_{ds}) \quad (10)$$

where  $i_{ds}, i_{qs}$  are the d-axis and q-axis current components of three combined stator currents, respectively;  $V_{ds}, V_{qs}$  are the d-axis voltage and q-axis voltage of the stator voltages, respectively;  $\lambda_{ds}, \lambda_{qs}$  are the d-axis flux and q-axis flux, respectively; and  $T_e$  is motor's electromagnetic torque.

In order to produce maximum torque, optimal operation is achieved by vector control, which ensures that the stator-current space vector contains only a quadrature component by considering  $i_{ds} = 0$ . As a result, the torque equation becomes

$$T_e = \frac{3}{2} p \lambda_m i_{qs} \quad (11)$$

Thus, the torque can be controlled directly by the current  $i_{qs}$  only. This approach is similar to the DC motor equation in which the torque is proportional to the winding current.

Since speed is directly related to torque, and torque is directly related to the q-axis current, motor speed can be controlled by varying the q-axis current. Note that current along the magnetic field of the rotor generates additional flux that may be converted to heat if it isn't needed to drive the rotor. This heat is wasted energy; it can be minimized by properly controlling the d-axis current.

In order to determine the d and q axis currents, the phase currents must be measured. Then, to transform these currents into the rotor frame, the rotor angle must be measured. Therefore, the electronics requires current sensors, plus an encoder attached to the rotor shaft to measure the rotor angle.

The steps necessary for vector control are detailed in Figure 3. As shown, the speed command is an input to the vector control method. On the right-hand side of the diagram, the vector-control electronics outputs PWM commands for the inverter, which is connected to the motor. Two current sensors in the configuration measure the phase-U and phase-W currents. These sensors are connected to the ADC (analog-to-digital converter) built into the MCU. The motor also has an encoder mounted on its rotor to give the quadrature pulses **A** and **B**, as well as the zero synch pulse **Z**. All three of the rotor position signals are sent to the MCU's input-capture and timer/quadrature counter peripheral for making speed measurements.



The angle is zero count when the Z pulse occurs. From this point onwards it is given a certain count value as the quadrature counter is read. As shown in Figure 4b, the angle is 18 and 34 counts when it is read at consecutive times at the current loop rate. These counts are transformed into a proper angle value so that sine and cosine values can be computed for the Park transformation.

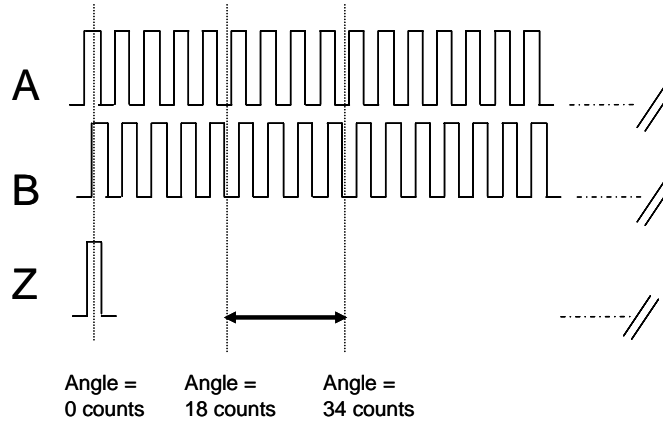


Fig. 4b Measuring rotor angle with encoder counts.

Motor speed determines how much the angle of the rotor changes over time. As shown in Figure 4c, pulses A and B from the encoder are used at the speed loop rate. Two angles are measured at constant time intervals, thus giving the measurements needed to compute speed: delta angle and delta time. Speed is computed by dividing the delta angle  $\Delta\theta$  by the delta time  $\Delta t$ .

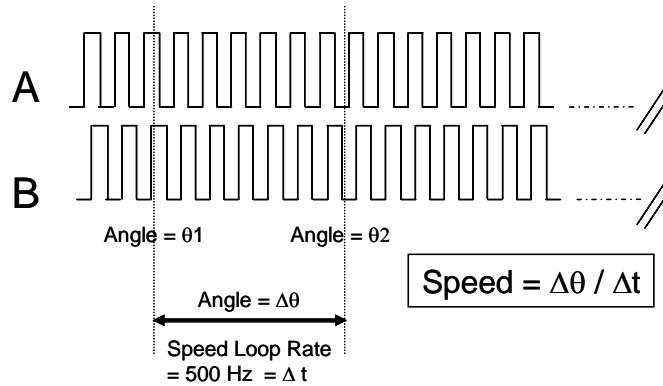


Fig. 4c Speed measurements using encoder pulses A and B at speed-loop rate.

The speed measurement and speed command are fed into the PI loop or auto-speed regulator (ASR, shown in Figure 3), which generates the reference q-axis current required to maintain the commanded speed. The reference q-axis current and the measured q-axis current are fed into the auto-current regulator (ACR) to create a q-axis voltage that is applied to the next PWM.

The reference current in the d-axis is generally maintained at a constant value to ensure proper flux in the stator. The reference d-axis current and the measured d-axis current are fed into a second ACR to create the d-axis voltage. Corrections are made to the voltage calculations

according to the number of pole pairs and the reference currents in the d and q axes. When the final values of  $V_d$  and  $V_q$  are computed, they are transformed from the rotor frame to the stator frame using an inverse transformation and the rotor angle value. Three voltages in the stator frame –  $V_u$ ,  $V_v$  and  $V_w$  – are converted into the PWM values that are output by the MCU's 3-phase timer unit.

Current measurements and ACR updates are executed at a current loop rate. This process, which is known as “inner loop,” uses the fastest control algorithm. A typical inner-loop rate is 4kHz or more. By contrast, encoder measurements — and especially speed measurements — are performed at a lower rate. Specifically, the ASR and related computations are performed using a slower process called “outer loop.” A typical encoder-based speed computation or outer loop rate is only about 500Hz, but it occasionally can drop to as low as 50Hz.

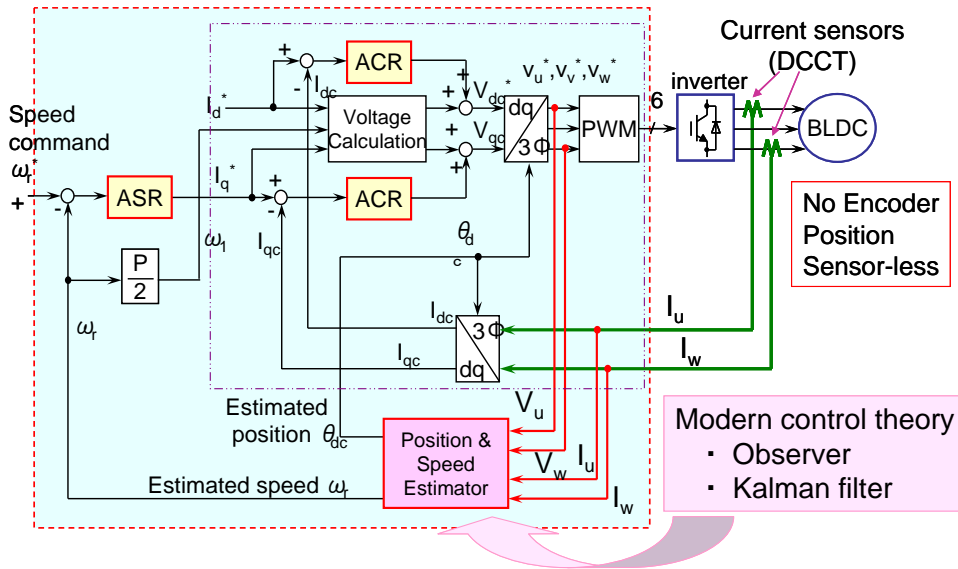
Vector control provides dynamic torque control based on exact speed measurements and current measurements. Consider an example in which the load changes during rotation. Since speed is measured several times per rotation (typically at a 500Hz rate), any load changes that affect the speed will be quickly detected. Then for the next rotation, the q-axis current will be adjusted properly to maintain the desired speed. If more current is required, the control circuit will supply it, and vice versa.

It's well accepted that the vector-control method does an excellent job of handling torque and flux, as well as accurately maintaining a desired speed. In fact, motion-control experts generally regard vector control as the reference against which the performance of other methods is compared and evaluated.

### **3. Sensorless Vector Control with DCCT Measurements**

Because the vector-control method just described requires a position sensor (encoder) and two current sensors, the final system configuration can be expensive. Consumer applications, especially white goods, are cost-sensitive and usually cannot afford this type of implementation. Fortunately, though, these applications require lower levels of performance and speed accuracy that can be met by two economical control methods: sensorless techniques that don't require position sensors. Both use the same 180-degree modulation and vector control algorithm [7,8,10].

The first of these methods eliminates the position sensor but keeps the two current sensors. Known as “DCCT-based sensorless vector control,” it is shown in Figure 5. Because this method uses no position sensor, angle and speed are estimated using the current measurements and voltages applied in the previous PWM cycle [10].



×Gain adjustment is very difficult.  
 (ASR, ACR ×2, Estimator(several parameters))

Fig. 5 Position-sensorless control with 2 DCCT current sensors

The estimation method employs a Kalman-filter approach based on principles of modern control theory, an observer-based model, and a state transition matrix [12]. Using the motor model described in section 2.1, the flux and angle can be calculated by applied voltages and measured currents. In the  $\alpha\beta$  frame, the motor model can be described as follows:

$$v_\alpha = R_s i_\alpha + \frac{d\lambda_\alpha}{dt} \quad (12)$$

$$v_\beta = R_s i_\beta + \frac{d\lambda_\beta}{dt} \quad (13)$$

where  $i_\alpha, i_\beta$  are the  $\alpha$ -axis current and  $\beta$ -axis current of the stator currents, respectively;  $v_\alpha, v_\beta$  are the  $\alpha$ -axis voltage and  $\beta$ -axis voltage of the stator voltages, respectively;  $\lambda_\alpha, \lambda_\beta$  are the  $\alpha$ -axis flux and  $\beta$ -axis flux, respectively; and  $R_s$  is the stator resistance.

The magnetic field flux equations are given:

$$\lambda_\alpha = \Lambda_m \cos \theta_r + L i_\alpha \quad (14)$$

$$\lambda_\beta = \Lambda_m \sin \theta_r + L i_\beta \quad (15)$$

where  $\Lambda_m$  is the constant flux vector;  $L$  is the motor phase inductance; and  $\theta_r$  is the rotor position.

Therefore, the above equations show that the magnetic flux can be obtained from applied voltages and measured currents simply by integration as follows:

$$\lambda_{\alpha} = \lambda_{\alpha 0} + \int_0^t (v_{\alpha} - R_s i_{\alpha}) dt \quad (16)$$

$$\lambda_{\beta} = \lambda_{\beta 0} + \int_0^t (v_{\beta} - R_s i_{\beta}) dt \quad (17)$$

where,  $\lambda_{\alpha 0}$   $\lambda_{\beta 0}$  are the initial values of the  $\alpha$  -axis flux and  $\beta$  -axis flux, respectively.

Furthermore

$$\Lambda_m \cos \theta_r = \lambda_{\alpha} - Li_{\alpha} \quad (18)$$

$$\Lambda_m \sin \theta_r = \lambda_{\beta} - Li_{\beta} \quad (19)$$

Because the phase inductance  $L$  is normally small, the inductance contribution in the above equation can be ignored. Therefore

$$\lambda_{\alpha} = \Lambda_m \cos \theta_r \quad (20)$$

$$\lambda_{\beta} = \Lambda_m \sin \theta_r \quad (21)$$

So the rotor phase can be deduced from the flux components as follows:

$$\theta_r = \text{tg}^{-1} \left( \frac{\lambda_{\beta}}{\lambda_{\alpha}} \right) \quad (22)$$

Position estimation is calculated through the low-pass filters and a derivation in order to remove the integration error and DC offset according to the flux equations:

- First low-pass filter
- Derivative
- Last low-pass filter

Speed estimation is obtained from the phase difference and then filtered with a third-order low-pass filter built from three first-order low-pass filters in series.

Estimated angle and speed are used together in the same vector-control algorithm to control the current in the q-axis. This implementation requires many matrix calculations. Thus it necessitates a fast MCU with high computing capability. The encoder has been eliminated from the system, so an on-chip timer isn't required for speed measurement. However, the task of angle and speed estimation consumes more CPU bandwidth.

Using an MCU from the Renesas SH-2 family [13], sensorless vector control has been developed and implemented. Our hardware reference platform for sensorless vector control is shown in Figure 6. This platform consists of two boards, a Renesas SH-2 series MCU RSK and a power board. The power board has AC-to-DC conversion and an integrated power module (IPM) with six power switches with built-in drivers. The heat dissipated by the IPM necessitates the heat sink shown in Figure 6.

To measure the motor currents in the U and V phases, the power board provides three DCCT devices. Three back-EMF resistor ladders plus a fourth resistor ladder for measuring the Vbus are also on the board. A precision shunt resistor on the low-voltage side is included to measure the overall current or to enable the one-shunt current detection (OSCD) technique for current

measurements. Rotor position and speed are estimated from the measured phase currents and the reference voltages. Together, these elements allow implementations of sensorless vector control algorithms.

The sensorless vector control design starts up in an open speed loop and closed current loop. The startup current and startup time vary, depending on the type of motor being driven and its load. During the open-loop startup phase, the rotor position and speed are estimated. At the conclusion of the startup time, the sensorless vector control immediately switches into the closed-loop speed control mode, using the estimated position and speed. The startup procedure is in the PWM interrupt.

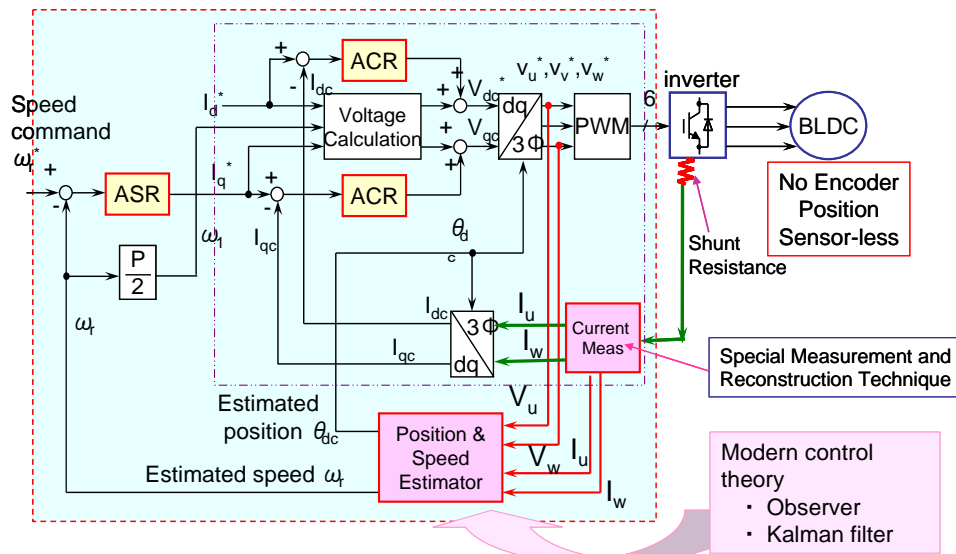


Fig. 6 Sensorless vector control implementation platform with current sensors from LEM USA.

The performance measurement setup used in our lab to evaluate the performance of DCCT based vector control consisted of a Renesas hardware platform driving a Bodine three-phase BLDC motor connected to a dynamometer. The test results are summarized in section 5.

#### 4. Sensorless Vector Control With One-shunt Current Detection Method

The vector control with one-shunt current detection (OSCD) method — also called “one-shunt current detection vector control” or simply “OSCD vector control” — eliminates the position sensor and two DCCT sensors. As Figure 7 shows, it measures two currents using one shunt resistance installed on the low side of the inverter. This precision resistor must be capable of handling the full current range of the motor. The implementation illustrated in Figure 7 is similar to that of the DCCT method, but adds one more computing block: Current Measurement. A closer look at the current measurement technique explains why this addition is necessary.



×Gain adjustment is very difficult.  
 (ASR, ACR ×2, Estimator(several parameters))

Fig. 7 OSCD implementation flow with current measurement module.

The implementation of sensorless vector control with OSCD is similar to the control method that measures currents using the transducers from LEM USA except that the current-reconstruction algorithm has to be developed and added. Figure 8 illustrates how to implement OSCD using two MTU2/2S timer channels of an SH-2 series microcontroller and the MCU's hardware-triggered ADC channels. In this figure, the W phase has the largest PWM value, the V phase has the next smaller value, and the U phase has the smallest value.

If the shunt current is measured between the rising edges of the W phase and V phase, we can conclude that the W phase current is measured. Based on PWM values, only the W phase (that is, only the Wp—upper W phase IGBT) is on at that time. Therefore, any current measured by the shunt resistor is the W current only. Next, if current is measured between the rising edges of the V phase and U phase, then the sum of both the W phase and V phase currents is measured. Additionally, the U phase current can be determined from this measurement because the sum of all three motor phase currents is zero. These current measurements must be performed at precise times during the PWM interrupt. To trigger the ADC channels at the precise time, two timer channels are used: MTU2S4.TADCOBRA and MTU2S4.TADCOBRB. Exact timer counts for these two channels are calculated based on the duty cycle, which is the known output of the control method.

The SH7080 MCU provides nine multi-function 16-bit timer pulse channels: six in MTU2 and three in the MTU2S. In our implementation, the MTU2S4.TADCOBRA and MTU2S4.TADCOBRB timer channels are assigned for one-shunt current timers that trigger ADC channels AN0 and AN6 at precisely the correct time, based on the PWM duty values of each phase.

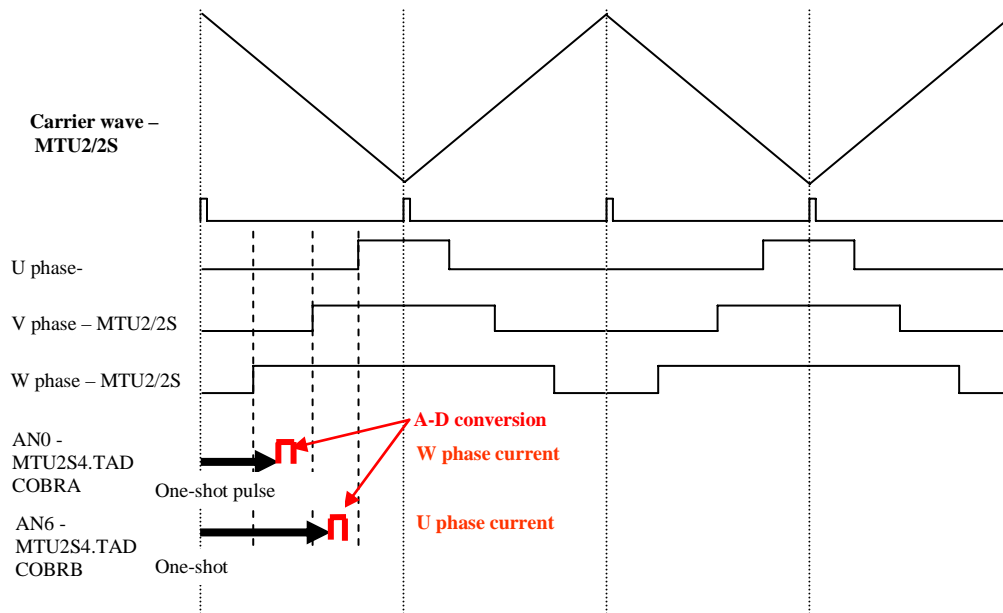


Fig. 8 One-shunt current detection using the MTU2 and MTU2S timer channels.

As part of this process, the PWM duty values of all three phases are compared to determine exactly how much time delay must be loaded into the MTU2S4.TADCOBRA and MTU2S4.TADCOBRB timer channels. It is important to note that the three PWM duty values are constantly changing, so that the W PWM count is not always the largest. The electronics has to determine which PWM duty value is the biggest each time, then use that value to set the proper flags for the phase for which current measurement is being performed.

Making the requisite PWM count comparisons, setting the flags for the phase, identifying the triggered ADC channel, and the other tasks required by this method necessitate complex processing that adds a significant amount of code and imposes an additional time/bandwidth load on the CPU compared to the control methods previously described. The CPU bandwidth required, for example, exceeds that of the sensorless vector control method that uses the LEM current sensors. Fortunately, ADC channels AN0 and AN6 are triggered by the MCU's hardware rather than software, saving code and shortening the ADC conversion time. Furthermore, the SH7080 MCU has great computing power, more than sufficient for the required processing, which makes OSCD implementation simpler and faster.

The lab setup we used to evaluate the performance of the sensorless vector control method with OSCD (one-shunt current detection) was nearly identical to the test setup previously described for evaluating the performance of the DCCT based vector control technique. The only change was the removal of the three LEM current sensors. Instead, the precision shunt resistance on the platform was used to obtain the data needed to reconstruct the motor phase currents (see Figure 9).

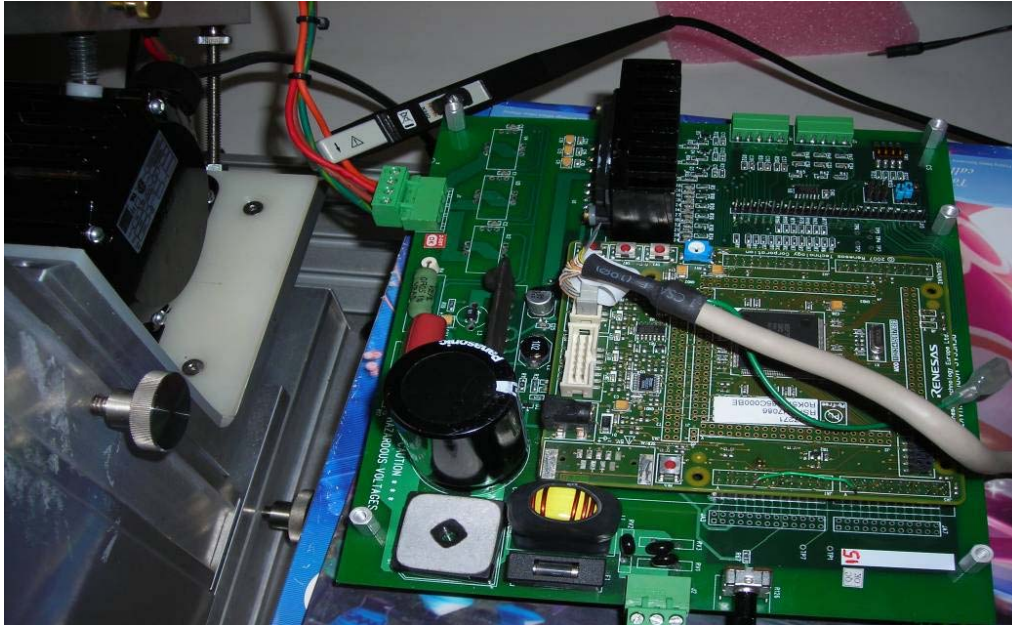


Fig. 9 Sensorless vector control implementation hardware platform with precision shunt resistor.

## 5. Comparison of Two Techniques for Speed Control

As previously mentioned, to better understand the theoretical analysis of the sensorless vector control methods described above, we performed experiments to compare the performance of sensorless vector control with LEM current sensors to that of the one-shunt current detection method. Evaluations were made in terms of cost, CPU resources (especially bandwidth) used, motor current, speed responses and regulations, and torque capability over the entire speed range — with and without full loads. The dynamometer was set up with a three-phase BLDC motor, brake (max torque 3.25Nm, max speed 15,000rpm), and Magtrol DSP6001 dynamometer controller. Three basic cases were compared:

- Case 1: Cost and CPU resources and bandwidth
- Case 2: Motor phase current — with and without load
- Case 3: Speed regulation and response.

### 5.1 Comparison of Cost and CPU Bandwidth

Compared to the DCCT-based sensorless vector control with the LEM sensors, the OSCD sensorless vector control with one shunt reduces cost, which is especially beneficial for home appliance applications. It removes two current sensors and related circuits. Even for the DCCT-based sensorless vector control with the LEM sensors, the shunt for DC bus current is still necessary as a safety precaution.

In terms of MCU resources, both control methods require nearly the same set of peripherals: two ADC channels, six PWM outputs, a timer with hardware dead-time insertion, and automatic emergency shutdown of PWM output from an external input.

For DCCT vector control, currents are measured by sensors on the high side of the power rail and these currents can be measured at any time. Typically, the currents are measured by triggering ADC channels at the peak of the PWM cycle. At this instance, all upper power switches are ON, so there should not be any PWM transients.

For OSCD-based vector control, though, currents must be measured at a precise time during the PWM cycle. This requires two more synchronous timer channels. Fortunately, various MCUs in the SH-2 series have MTU2 + MTU2s timer channels with the requisite resources.

With regard to CPU bandwidth, one-shunt current reconstruction is somewhat complicated, and it uses a bit more CPU bandwidth than DCCT vector control.

Table I, below, compares the LEM-based and OSCD-based methods of sensorless vector control. [11]

Table I Comparison of control methods in terms of CPU bandwidth and approximate costs.

Control Method	MCU Used	Test Conditions	Bandwidth	Control Performance ( $\pm 20\%$ load variation)	Ballpark Cost for Speed-Control MCU & Sensor(s) (10k units)	Comments
Vector control without encoder	SH7086 running at 80MHz	Inner and outer loops running at 10KHz	21.2MHz for SH7086 (RISC)	$\pm 2-4\%$	16 or 32-bit MCU: ~\$6 to \$20 2 DCCTs: ~\$6-\$12	Accurate control & good dynamic performance; requires more CPU computing
Vector control with one-shunt current detection		Inner loop running at 10KHz	22.8MHz for SH7086 (RISC)	$\pm 2-4\%$	16 or 32-bit MCU: ~\$6 to \$20 Shunt resistors: <\$1 each	Accurate control & good dynamic performance; requires more CPU computing

The sensorless vector control method does not use an encoder for angle and speed measurements. Instead, it uses an estimation technique based on a Kalman filter. As a result, the control software has to perform additional tasks at the same rate as the inner loop. Because of this, the bandwidth calculations are simple and directly proportional to the inner loop rate. For our implementation using an SH7086 RISC MCU, we selected a 10kHz inner loop frequency and chose the same PWM frequency for simplicity. The following data show the execution times for each main module of sensorless vector control with the LEM.

<b>Tasks</b>	<b>SH7086</b>
Current measurements	<b>7.2<math>\mu</math>s</b>
Flux & speed estimation	<b>12.75<math>\mu</math>s</b>
Angle estimation	<b>1.75<math>\mu</math>s</b>
Vector computations (matrix transformations)	<b>3.1<math>\mu</math>s</b>
Current loop	<b>3.75<math>\mu</math>s</b>
Speed loop	<b>1.6<math>\mu</math>s</b>
Overall measurements	<b>33.15<math>\mu</math>s</b>

With the sensorless vector control with OSCD method, ADC measurements have to be made at a specific time during PWM execution. To control the ADC trigger and convert the raw ADC counts to current measurements, the MCU must perform additional software tasks. For the one-shunt current measurements, the shunt current is read through the hardware ADC trigger, so time isn't wasted waiting for the ADC conversion in poll mode. In fact, we found that the current measurement takes only 1.75 $\mu$ s. Execution times for several other tasks were also determined, as shown in the list below. (To simplify this task, in several places in the overall software configuration we used code size to estimate the execution time required to identify which currents were measured according to PWM values.)

<b>Tasks</b>	<b>SH7086</b>
Current measurements	<b>1.75<math>\mu</math>s</b>
Flux & speed estimation	<b>8.75<math>\mu</math>s</b>
Angle estimation	<b>1.75<math>\mu</math>s</b>
Current loop	<b>3.75<math>\mu</math>s</b>
Speed loop	<b>1.6<math>\mu</math>s</b>
ADC index tracking per PWM (estimated)	<b>2.5<math>\mu</math>s</b>
Overall measurements	<b>35.65<math>\mu</math>s</b>

From the CPU bandwidth measurements, we observed that the OSCD vector-control method takes additional CPU bandwidth, as expected. However, the increase was quite small: less than ten percent.

## 5.2 Comparison of Motor Phase Currents

Figures 10 and 11 show the motor phase current with and without load at 1000rpm for sensorless vector control with OSCD and with LEM current sensors. The current waveforms in both figures are similar. The current is sinusoidal at 1000rpm. It is very low without load, and then increases to 1.5A current at 0.5Nm load. Our test results demonstrated that sensorless vector control exhibits very good field-oriented control and that the rotor position was estimated correctly.

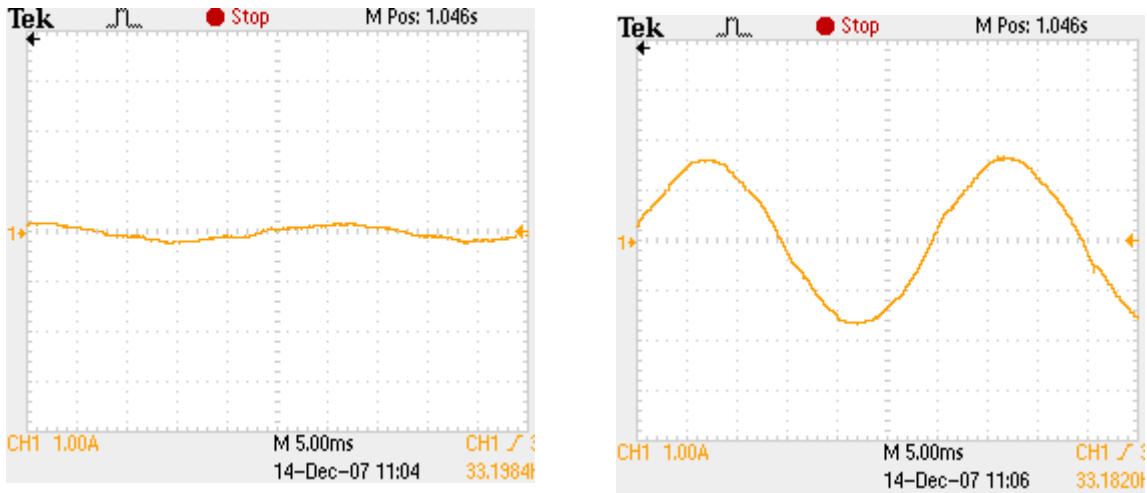


Fig. 10 Motor phase current at 1000rpm without load (left) and with 0.5Nm load (right) for sensorless vector control with one-shunt current detection.

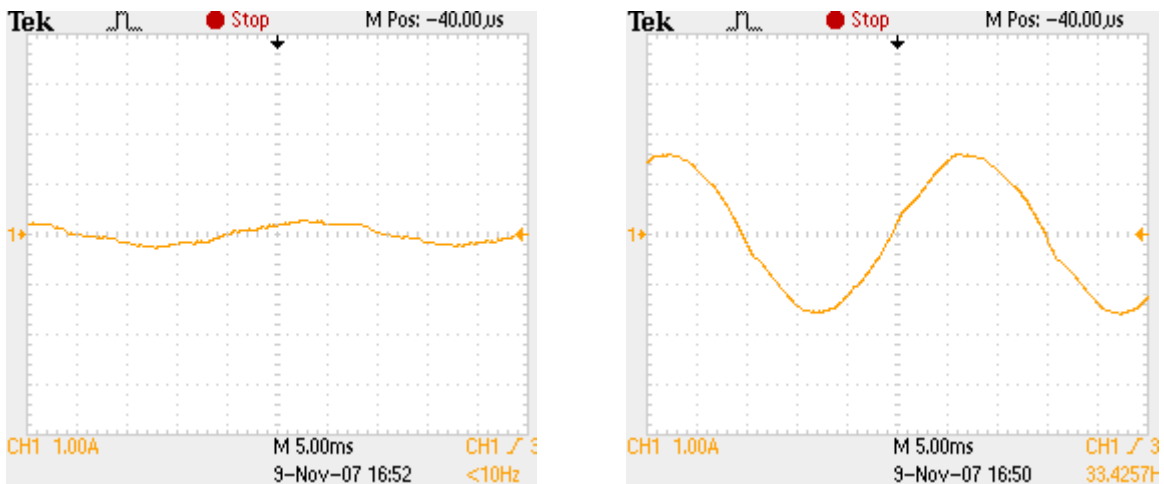


Fig. 11 Motor phase current at 1000rpm without load (left) and with 0.5Nm load (right) for sensorless vector control with LEM current sensors.

### 5.3 Comparison of Speed Response and Regulation

Figures 12 and 13 show speed and torque curves with 0.5Nm step load at 2000rpm for sensorless vector control methods with OSCD and LEM current sensors, respectively. To determine transient response, we added and removed the load on the motor. In both cases, the rotor speeds were observed to quickly return to the reference speed when the load changes were very stable.

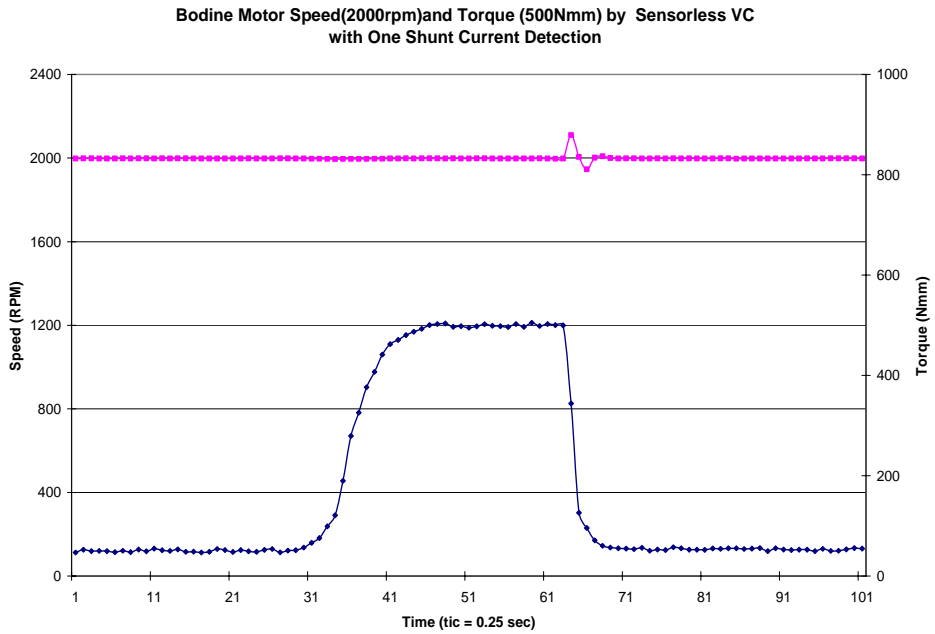


Fig. 12 Motor speed (2000rpm) vs. torque (0.5Nm) for sensorless vector control with one-shunt current detection.

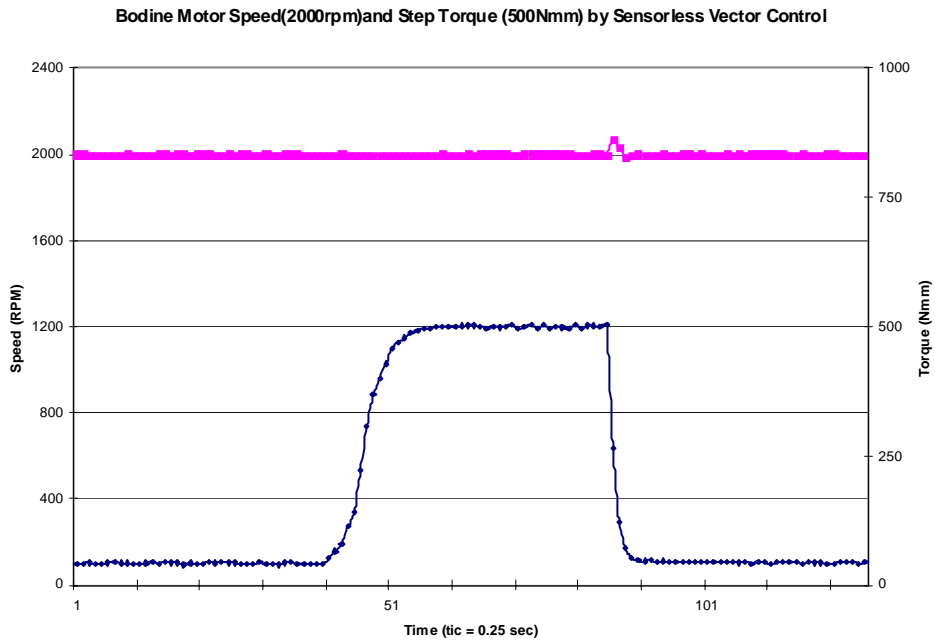


Fig. 13 Motor speed (2000rpm) vs. torque (0.5Nm) for sensorless vector control with LEM current sensors.

When a load is applied or removed, the sensorless control method responds very well and handles the speed decrease or increase appropriately. Estimation of angle and speed is very good because there is no loss of synchronization.

## 6. Summary

This paper has described sensorless vector control technology and its implementation. We introduced the BLDC motor and basic vector control theory, then discussed the modeling and control strategy of sensorless vector control of BLDC motors with (1) LEM current sensors and (2) OSCD. We compared two sensorless vector control techniques — DCCT-based vector control and OSCD-based vector control — in terms of the CPU bandwidths required, current profiles with and without loads, and speed regulation. Torque capability was tested and demonstrated using dynamometer tests. The comparison data and test results have demonstrated that both of the sensorless vector control methods achieve similar levels of high dynamic and steady-state performance.

Encoder-based vector control requires an encoder and two current sensors. The cost of these sensor components can range between \$14 and \$25, depending on the resolution of the encoder and the current measurement capability. By eliminating the encoder from a motor design, cost can be reduced by from about \$6 to \$12. This savings is significant in cost-sensitive applications. Furthermore, when DCCT sensors are eliminated and the single shunt resistor is used, the cost can be reduced even further, to less than \$2. The OSCD approach is therefore especially suitable for applications that are very cost-sensitive.

Note that we have not attempted to compare the performance of sensorless vector control to that of scalar control. However, many experts agree that either of the sensorless control methods offers better performance, because the scalar control method cannot handle dynamic load changes.

## References

- [1] T. Miller, "Brushless PM and Reluctance Motor Drives," Oxford, UK. Clarendon, 1989
- [2] B.K. Bose, "Power Electronics and Variable Frequency Drives," Piscataway, NJ. IEEE Press, 1996
- [3] P. Vas, "Sensorless Vector and Direct Torque Control," Oxford Science Publications, New York, 1998.
- [4] D. Novotny and T.A. Lipo, "Vector Control and Dynamics of AC Drives," Oxford University Press, New York, 1996.
- [5] Stefano Frattesi, and Luca Pasqualini, "A Three-Phase Motor Drive for Domestic Washing Machines", IEEE Proc. International Appliance Manufacturing, 2004, Issue 8, pp. 146-152.
- [6] Cho, K. Y., Yang, S. B., and Hong, C. H., "Sensorless Control of A PM Synchronous Motor for Direct Drive Washer without Rotor Position Sensors", IEEE Proc. Electric Power Applications, 2004, Vol. 151, Issue 1, pp. 61-69.
- [7] P. Vas, "Vector Control of AC Machines," Clarendon Press, New York, 1990.
- [8] J. P. Johnson, M. Ehsani and Y. Guzelgunler, "Review of sensorless methods for Brushless DC," in conf. Rec. IEEE-IAS Annual Meeting, vol. 1, 1999, pp. 143 – 150.
- [9] Yashvant Jani, "Implementing Embedded Speed Control for Brushless DC Motors," part 2, ESC conference, San Jose, 2006.
- [10] Yashvant Jani, "Implementing Embedded Speed Control for Brushless DC Motors, part 1," ESC conference, San Jose, 2006.
- [11] Kevin King; Robert Proctor; Huangsheng Xu, and Yashvant Jani, "MCU Performance for Various Control Algorithms of BLDC Motors," e-Drive conference, Atlanta, 2008.
- [12] Renesas internal application notes: "Sensorless Vector Control of PMSM Motors," San Jose, 2008.
- [13] SH7080 Group hardware manual, Renesas 32-bit RISC Microcomputer Super H RISC engine family , document REJ09B0181-0200, Japan, 2006

## About the Authors

**Yashvant Jani**, director of applications engineering, is currently involved in developing advance motor control applications. He has more than 15 years experience in embedded systems applications, the last four plus years of which has been in motor control, particularly the development and testing of vector control methods for BLDC motors. He is the author of “Implementing Embedded Speed Control for BLDC Motors” seminars offered at ESC in 2006 and 2007, and has taught networking and VoIP seminars at ESC in the 1999-2001 time frame. Jani received his Ph.D. in Physics from University of Texas at Dallas (UT-D) in 1976 and worked for the space shuttle program for fifteen years in systems for integrated guidance, navigation and control.

**Huangsheng Xu** received a Ph.D. degree in electrical engineering from Texas A&M University, College Station, Texas, in 2001. In the past ten years he has been working in the field of motor drives and power electronics. He holds three U.S. patents and has published over ten papers in the IEEE journals and conference proceedings. Currently he is working at Renesas Technology America on solutions for motor control applications.